Electronic Supplementary Material (ESI) for Inorganic Chemistry Frontiers.

Teach an old molecule new tricks: evidence and rationalisation of a slow dynamics of magnetisation in $[DyTp_2Acac]^{\dagger}$

Guégan Frédéric [1,2,*,‡], Riobé François [3], Maury Olivier [3], Jung Julie [4], Le Guennic Boris [4], Morell Christophe [2] and Luneau Dominique[1,*]

[1] Univ Lyon, Université Claude Bernard Lyon 1, CNRS, Laboratoire des Multimatériaux et Interfaces, F-69622, Villeurbanne, France.
‡Present address: Sorbonne Université, CNRS, Laboratoire de Chimie Théorique, LCT, F-75005 Paris, France.
[2] Univ Lyon, Université Claude Bernard Lyon 1, ISA (Institut des Sciences Analytiques de Lyon) – CNRS UMR 5280, F-69100, Villeurbanne, France.
[3] Univ Lyon, Ens de Lyon, CNRS UMR 5182, Université Claude Bernard Lyon 1, Laboratoire de Chimie, F69342 Lyon, France.
[4] Univ Rennes, CNRS, ISCR (Institut des Sciences Chimiques de Rennes) - UMR 6226, F-35000 Rennes, France.

Ab initio calculation results

Basis set dependence

Basis set dependence of the outcome of the SA-CASSCF/RASSI-SO calculations was studied.[1–3] ANO basis sets from the ANO-RCC library were used,[4–6] with the following contractions:

- BS1: [8s7p4d3f2g1h] for Dy, [3s2p1d] for the C, N, B and O atoms, and [2s] for the H atoms.
- BS2: [8s7p4d3f2g1h] for Dy, [4s3p2d] for the N, O and B atoms, [3s2p1d] for the C, and [2s] for all the H atoms.
- BS3: [8s7p4d3f2g1h] for Dy, [4s3p2d] for all the B, C, N, O atoms, and [2s] for all the H atoms.

The calculated energy splitting and M_J decomposition of the doublets are given in Tables S1 to S3.

Table S1: Energies, Landé tensors and M_J decomposition of the $^6H_{15/2}$ doublets calculated with BS1.

Root	E (cm^{-1})	g_X, g_Y, g_Z	M_J decomposition
1	0.00	(0.01, 0.01, 19.70)	$0.97\|\pm 15/2\rangle$
2	102.99	(0.14, 0.20, 17.22)	$0.79\|\pm 13/2\rangle + 0.18\|\pm 11/2\rangle$
3	166.04	(0.74, 0.94, 13.49)	$0.46\|\pm 11/2\rangle + 0.40\|\pm 9/2\rangle$
4	226.88	(3.05, 4.66, 9.65)	$0.41\|\pm 7/2\rangle + 0.23\|\pm 9/2\rangle + 0.13\|\pm 5/2\rangle$
5	279.74	(0.16, 4.39, 9.78)	$0.28\|\pm 5/2\rangle + 0.27\|\pm 1/2\rangle + 0.21\|\pm 7/2\rangle + 0.17\|\pm 3/2\rangle$
6	323.65	(1.58, 5.17, 12.90)	$0.36\|\pm 3/2\rangle + 0.30\|\pm 5/2\rangle + 0.23\|\pm 1/2\rangle$
7	411.96	(0.02, 0.04, 19.78)	$0.28\|\pm 9/2\rangle + 0.23\|\pm 11/2\rangle + 0.21\|\pm 7/2\rangle + 0.12\|\pm 5/2\rangle$
8	510.27	(0.04, 0.08, 19.49)	$0.43\|\pm 1/2\rangle + 0.32\|\pm 3/2\rangle + 0.16\|\pm 5/2\rangle$

Table S2: Energies, Landé tensors and M_J decomposition of the $^6H_{15/2}$ doublets calculated with BS2.

Root	E (cm^{-1})	g_X, g_Y, g_Z	M_J decomposition
1	0.00	0.01 0.01 19.71	$0.97\|\pm 15/2\rangle$
2	107.45	0.13 0.18 17.20	$0.80\|\pm 13/2\rangle + 0.17\|\pm 11/2\rangle$
3	173.08	0.64 0.82 13.52	$0.48\|\pm 11/2\rangle + 0.39\|\pm 9/2\rangle$
4	236.13	3.04 4.51 9.63	$0.41\|\pm 7/2\rangle + 0.25\|\pm 9/2\rangle + 0.12\|\pm 5/2\rangle$
5	291.25	0.27 4.49 9.54	$0.28\|\pm 5/2\rangle + 0.27\|\pm 1/2\rangle + 0.22\|\pm 7/2\rangle + 0.15\|\pm 3/2\rangle$
6	336.37	1.60 5.21 12.89	$0.38\|\pm 3/2\rangle + 0.30\|\pm 5/2\rangle + 0.22\|\pm 1/2\rangle$
7	418.34	0.03 0.04 19.78	$0.28\|\pm 9/2\rangle + 0.22\|\pm 11/2\rangle + 0.21\|\pm 7/2\rangle + 0.12\|\pm 5/2\rangle$
8	523.36	0.04 0.08 19.49	$0.44\|\pm 1/2\rangle + 0.32\|\pm 3/2\rangle + 0.16\|\pm 5/2\rangle$

Table S3: Energies, Landé tensors and M_J decomposition of the $^6H_{15/2}$ doublets calculated with BS3.

Root	E (cm^{-1})	g_X, g_Y, g_Z	M_J decomposition
1	0.00	0.01 0.01 19.70	$0.97\|\pm 15/2\rangle$
2	107.60	0.12 0.17 17.18	$0.80\|\pm 13/2\rangle + 0.17\|\pm 11/2\rangle$
3	173.05	0.69 0.86 13.51	$0.49\|\pm 11/2\rangle + 0.39\|\pm 9/2\rangle$
4	236.30	2.88 4.42 9.67	$0.41\|\pm 7/2\rangle + 0.26\|\pm 9/2\rangle + 0.12\|\pm 5/2\rangle$
5	292.21	9.04 4.58 0.09	$0.28\|\pm 5/2\rangle + 0.26\|\pm 1/2\rangle + 0.23\|\pm 7/2\rangle + 0.15\|\pm 3/2\rangle$
6	336.86	1.69 5.61 12.60	$0.38\|\pm 3/2\rangle + 0.29\|\pm 5/2\rangle + 0.23\|\pm 1/2\rangle$
7	419.40	0.03 0.04 19.78	$0.28\|\pm 9/2\rangle + 0.22\|\pm 11/2\rangle + 0.21\|\pm 7/2\rangle + 0.13\|\pm 5/2\rangle$
8	522.54	0.04 0.08 19.48	$0.44\|\pm 1/2\rangle + 0.32\|\pm 3/2\rangle + 0.16\|\pm 5/2\rangle$

Thermal dependence of the relaxation rate

As described in the manuscript, the thermal dependance of the magnetisation relaxation rate was obtained through the fitting of the $\chi'' = f(\nu)$ curves at constant temperature, using

$$\chi'' = (\chi_T - \chi_S)\,\frac{(2\pi\nu\tau)^{1-\alpha}\cos(\pi\alpha/2)}{1 + 2(2\pi\nu\tau)^{1-\alpha}\sin(\pi\alpha/2) + (2\pi\nu\tau)^{2-2\alpha}}. \quad (1)$$

Fittings were performed using SciDavis,[7] and the χ_S and χ_T parameters were fixed to the values deduced from the fitting of the Cole-Cole plots at constant temperature. We provide in Table S4 the calculated χ_S, χ_T and α parameters from these fittings, the associated error bars and the R^2 factor. We then provide in Table S5 the α and τ parameters obtained *via* equation 1, the associated error bars and the agreement factors R^2. One may note the very good agreement in the α values from both procedures.

Finally, we give in Figure S1 the $\nu = f(T)$ and log-log representation of these data, and also the best fit obtained with $\nu = 1971(4) + 1.06(2)T^3$, R^2=0.996. One may note the error bars are rather moderate in the $\nu = f(T)$, and appear much larger in the log-log representation (distortion).

Table S4: Fitted parameters from the Cole-Cole $\chi'' = f(\chi')$ plots, associated error bars and agreement factor R^2 for each temperature.

T (K)	$\alpha \pm \Delta\alpha$	$\chi_T \pm \Delta\chi_T$ (cm^3/mol^{-1})	$\chi_S \pm \Delta\chi_S$ (cm^3/mol^{-1})	R^2
2.0	0.09 ± 0.01	4.183 ± 0.008	0.44 ± 0.04	0.995
2.4	0.09 ± 0.02	3.657 ± 0.006	0.39 ± 0.04	0.994
2.8	0.09 ± 0.02	3.193 ± 0.005	0.35 ± 0.03	0.995
3.2	0.09 ± 0.02	2.810 ± 0.004	0.31 ± 0.03	0.995
3.6	0.09 ± 0.02	2.504 ± 0.004	0.27 ± 0.03	0.995
4.0	0.09 ± 0.01	2.247 ± 0.003	0.25 ± 0.02	0.996
4.4	0.08 ± 0.02	2.021 ± 0.003	0.24 ± 0.02	0.993
4.8	0.08 ± 0.02	1.855 ± 0.002	0.22 ± 0.02	0.995
5.2	0.07 ± 0.02	1.717 ± 0.003	0.21 ± 0.02	0.993
5.6	0.08 ± 0.01	1.598 ± 0.002	0.19 ± 0.02	0.996
6.0	0.07 ± 0.01	1.489 ± 0.002	0.18 ± 0.02	0.994
6.4	0.07 ± 0.02	1.398 ± 0.002	0.17 ± 0.02	0.994
6.8	0.07 ± 0.01	1.318 ± 0.001	0.17 ± 0.01	0.996
7.2	0.06 ± 0.02	1.242 ± 0.002	0.16 ± 0.02	0.993
7.6	0.06 ± 0.01	1.180 ± 0.001	0.16 ± 0.01	0.996
8.0	0.05 ± 0.01	1.120 ± 0.001	0.15 ± 0.01	0.995

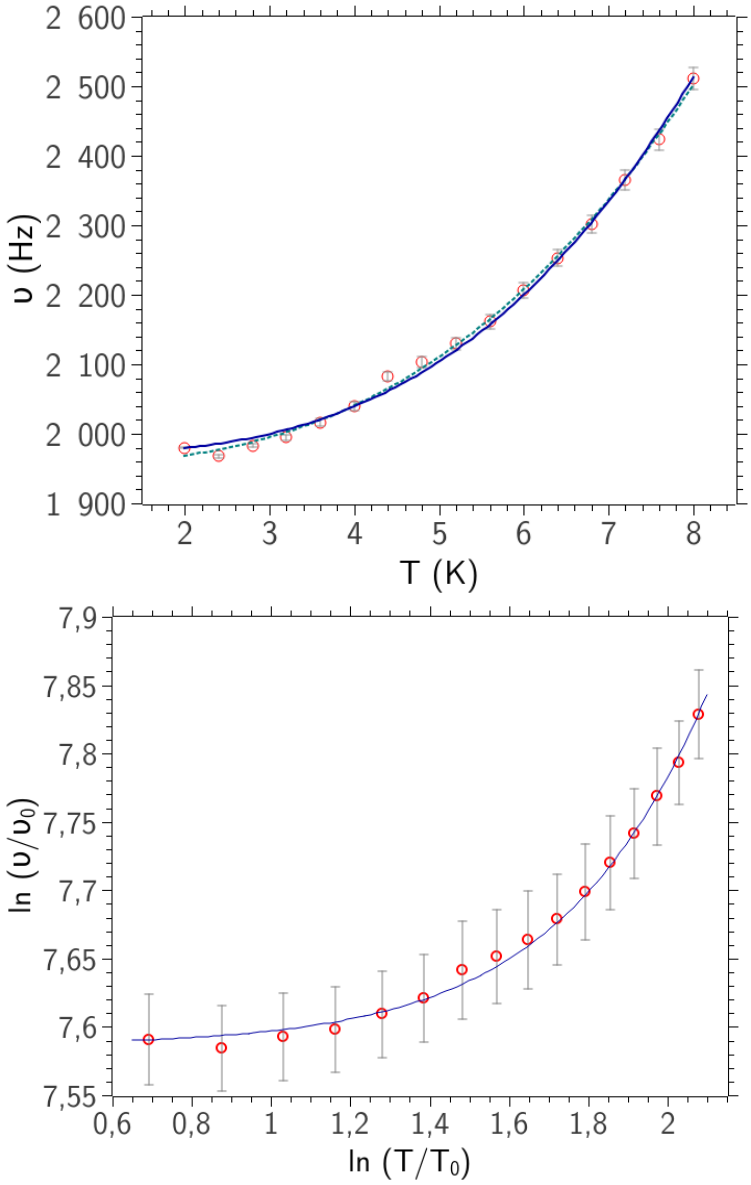

Figure S1: ○, thermal dependence of the relaxation frequency as deduced from the fittings of the $\chi'' = f(\nu)$ curves at constant temperature, with associated error bars (in gray). –, calculated values from the best fit of the $\nu = f(T)$ curve ($\nu = 1971(4) + 1.06(2)T^3$, R^2=0.996). Top panel: $\nu = f(T)$ plot; bottom panel: log-log plot.

Table S5: Fitting parameters from equation 1, associated error bars and agreement factor R^2 for each temperature. Frequencies are also given.

T (K)	$\alpha \pm \Delta\alpha$	$\tau \pm \Delta\tau$ (10^{-4}s)	$\nu \pm \Delta\nu$ (Hz)	R^2
2.0	0.09 ± 0.01	5.1 ± 0.2	1980 ± 67	0.989
2.4	0.09 ± 0.01	5.1 ± 0.2	1968 ± 63	0.994
2.8	0.09 ± 0.01	5.0 ± 0.2	1983 ± 65	0.993
3.2	0.09 ± 0.01	5.0 ± 0.2	1995 ± 63	0.994
3.6	0.10 ± 0.01	5.0 ± 0.2	2017 ± 64	0.994
4.0	0.09 ± 0.01	4.9 ± 0.2	2040 ± 66	0.994
4.4	0.08 ± 0.02	4.8 ± 0.2	2082 ± 76	0.992
4.8	0.08 ± 0.01	4.8 ± 0.2	2104 ± 74	0.992
5.2	0.08 ± 0.02	4.7 ± 0.2	2130 ± 78	0.992
5.6	0.08 ± 0.01	4.6 ± 0.2	2161 ± 74	0.993
6.0	0.08 ± 0.01	4.5 ± 0.2	2206 ± 78	0.992
6.4	0.07 ± 0.01	4.4 ± 0.1	2253 ± 78	0.993
6.8	0.07 ± 0.01	4.3 ± 0.1	2302 ± 76	0.993
7.2	0.07 ± 0.01	4.2 ± 0.1	2365 ± 85	0.992
7.6	0.06 ± 0.01	4.1 ± 0.1	2423 ± 75	0.994
8.0	0.06 ± 0.01	4.0 ± 0.1	2511 ± 83	0.994

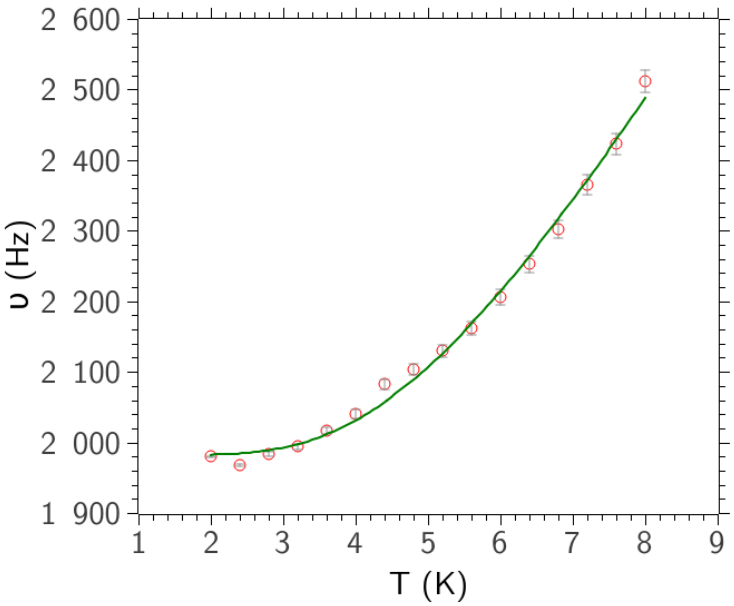

Figure S2: ○, thermal dependence of the relaxation frequency as deduced from the fittings of the $\chi'' = f(\nu)$ curves at constant temperature, with associated error bars (in gray). –, calculated values from the best fit of the $\nu = f(T)$ curve with $\nu = (5.2(6)\ 10^3)\exp(-19(1)/T) + 1982(7)$ Hz.

Additionnal AC SQUID data

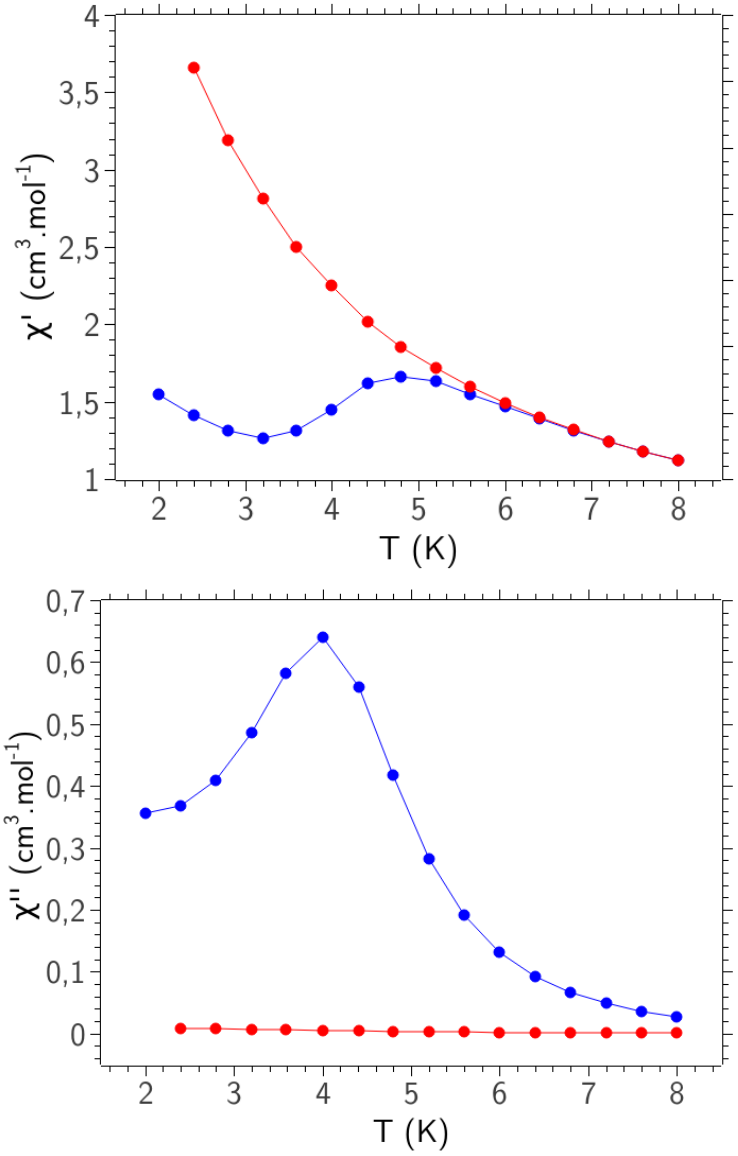

Figure S3: Top: $\chi' = f(T)$ at 1 Hz measured under a static field of 0 Oe (red bullets) and 500 Oe (blue bullets). Bottom: $\chi'' = f(T)$ at 1 Hz, measured under the same conditions.

Luminescence decay measurement

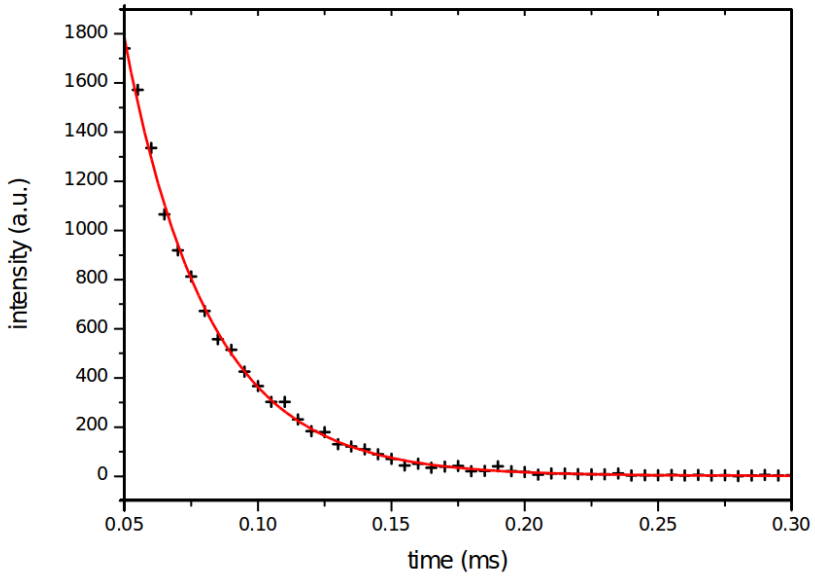

Figure S4: Luminescence decay measurement, under a 350 nm incident radiation, measured at 580 nm at ambient temperature. The red solid curve represents the best mono-exponential fit, $I = I_0 \exp(-t/\tau) + I_{res}$ with $I_{res} = 1(3)$, $I_0 = 8.8(2) \times 10^3$ (arbitrary units) and $\tau = 31.4(4)$ ms.

References

[1] Roos, B. O.; Taylor, P. R.; Siegbahn, P. E. M. *Chem. Phys.* **1980**, *48*, 157–173.

[2] Malmqvist, P. A.; Roos, B. O.; Schimmelpfennig, B. *Chem. Phys. Lett.* **2002**, *357*, 230–240.

[3] Malmqvist, P. A.; Roos, B. O. *Chem. Phys. Lett.* **1989**, *155*, 189–194.

[4] Roos, B. O.; Lindh, R.; Malmqvist, P.-A.; Veryazov, V.; Widmark, P.-O. *J. Phys. Chem. A* **2004**, *108*, 2851–2858.

[5] Roos, B. O.; Lindh, R.; Malmqvist, P.-A.; Veryazov, V.; Widmark, P.-O. *J. Phys. Chem. A* **2005**, *109*, 6575–6579.

[6] Roos, B. O.; Lindh, R.; Malmqvist, P.-A.; Veryazov, V.; Widmark, P.-O.; Borin, A. C. *J. Phys. Chem. A* **2008**, *112*, 11431–11435.

[7] Benkert, T.; Franke, K.; Narayanankutty, A.; Pozitron, D.; Standish, R. SciDavis 1.22. http://scidavis.sourceforge.net/, 2017.